Modeling and Analysis of Cavity Antennas on Cylindrical Ground Planes

Dennis J. Duven

The gain and phase properties of horizontally and vertically oriented cavity antennas on cylindrical ground planes are modeled and analyzed. These antennas are frequently used on missiles to receive or transmit the signals of interest. Since many electronic measurement systems now use the phase of the signals as a sensitive ruler for measuring distances and velocities, an accurate understanding of the phase properties of cavity antennas is required.

INTRODUCTION

Many modern electronic measurement systems are now using the phase of electromagnetic signals propagated between components of the system as electronic rulers for measuring distances and velocities. The Global Positioning System (GPS) is an important example of such a measurement system.[1] The GPS is composed of 24 satellites that orbit the Earth in a set of six circular rings at a nominal radius of 26,559.8 km from the center of the Earth. Each satellite radiates a pair of phase-modulated radio frequency (RF) carriers that are received by the navigation receivers located in the vehicles to be navigated. The navigation receivers have signal and data processing capabilities that enable them to measure the propagation time of the signals received from the GPS satellites (and therefore also the range or distance of the satellites from the navigation receiver), and then calculate the location of the receiver from the satellite-to-receiver range measurements and the known positions of the satellites.

The propagation time measurements are taken by using delay-locked loops to synchronize receiver-generated, time-shifted replicas of the satellite modulation codes with the signals received from the satellites. The time shifts required to achieve synchronization on each satellite are then measures of the propagation times of the signals from each satellite. These measurements typically have noise levels with standard deviations of 0.3–3.0 m, depending on how the delay-locked loops are implemented. Ambiguous satellite-to-receiver range measurements with noise levels of only a few millimeters can also be generated by using phase-locked loops to accomplish similar phase lock of receiver-generated carriers with the received carriers. These measurements are ambiguous because the RF carriers are periodic, and every cycle looks like every other cycle. However, if the receiver is properly designed and takes full advantage of all the information provided by the GPS signals, it is possible to resolve the ambiguities (i.e., determine

which cycle is the correct cycle) and thereby provide unambiguous range measurements with noise levels of only a few millimeters. When these phase-derived range measurements are used to compute navigation solutions, the position estimates obtained have noise levels that are typically only a few centimeters.

The accuracy of the navigated solutions also depends on how well the systematic error sources are modeled and corrected. The phase pattern of the antenna used to receive the GPS signals is one of the important sources of systematic error. Navigation programs typically model the range and phase measurements as if they were obtained from a zero-size antenna located at a point called the "phase center" of the antenna. Real antennas, however, do not have zero size, and the effective phase center depends on the direction of arrival of the incoming signals and is therefore different for each satellite. To correct for this, the phase pattern of the antenna relative to a specified reference point in or near the antenna is defined and evaluated for all directions of arrival, either by measurement or by mathematical modeling.[2] This phase pattern is then used to adjust the measured range and phase data so that they appear to have been obtained from an ideal zero-size antenna at the specified reference point.

When the vehicle being navigated is a missile, the cylindrical shape and metallic composition of the missile's body substantially influence the phase behavior of whatever type of antenna is used. The antenna of choice has traditionally been a microstrip ring antenna because it provides approximately spherical coverage and is more predictable in phase than other types of antenna systems (e.g., two or more summed, and therefore interfering, sets of cavity antennas). However, microstrip ring antennas are physically large and not as predictable in phase as they need to be to take full advantage of the low-noise-level capability of the phase-processing receivers. Therefore, it is currently believed that three or more commutated (and therefore noninterfering) small antennas such as cavity or microstrip patch antennas would be more suitable. However, these antennas are still influenced by the ground plane to which they are attached, and a theoretical understanding of what these effects are is needed. The results of an investigation into the gain and phase properties of horizontally and vertically oriented cavity antennas on cylindrical ground planes are presented in this paper. It is anticipated that a similar study of the properties of microstrip patch antennas on cylindrical ground planes will be conducted in the near future.

THEORY

Equations defining the RF fields produced by cavity antennas mounted on large circular cylinders were published in 1955 in the *IRE Transactions on Antennas and Propagation*,[3] and are reproduced below. If the cavity is horizontal (i.e., its long axis is parallel to the circumference of the missile), then the electromagnetic field (E field) produced by the cavity is given by the following two equations:

$$E_\theta = -j2AV_0ka\left(\frac{1}{\sin\theta}\right)$$
$$\times \sum_{n=0}^{\infty}\left[\frac{\epsilon_n j^n \cos(n\varphi)}{H_n^{(2)}(ka\sin u)}\frac{\cos\left(\frac{n\pi}{2ka}\right)}{(ka)^2 - n^2}\right], \quad (1)$$

and

$$E_\varphi = -j2AV_0ka\left(\frac{\cos\theta}{ka\sin^2\theta}\right)$$
$$\times \sum_{n=1}^{\infty}\left[\frac{2nj^n \sin(n\varphi)}{\dot{H}_n^{(2)}(ka\sin\theta)}\frac{\cos\left(\frac{n\pi}{2ka}\right)}{(ka)^2 - n^2}\right], \quad (2)$$

where

$$A = \frac{1}{2\pi^2}\frac{e^{-jkR}}{R}, \quad (3)$$

and

$$j = \sqrt{-1}, \quad (4)$$

and

$$\epsilon_n = \begin{cases} 1, n=0 \\ 2, n>0 \end{cases}. \quad (5)$$

If the cavity is vertical (i.e., its long side is parallel to the axis of the missile), then the E field is given by the next two equations:

$$E_\theta = 0, \quad (6)$$

and

$$E_\varphi = \frac{2AV_0}{ka}\frac{\cos\left(\frac{\pi}{2}\cos\theta\right)}{\sin^2\theta}$$
$$\times \sum_{n=0}^{\infty}\frac{\epsilon_n j^n \cos(n\varphi)}{\dot{H}_n^{(2)}(ka\sin\theta)}. \quad (7)$$

In these equations, the spherical coordinates of the observation point defined in Fig. 1 are represented by $\{R, \theta, \varphi\}$, the radius of the cylinder is represented by a, the RF drive voltage across the center of the slot is represented by V_0, and the RF wavenumber is represented by k. The function $H_n^{(2)}(x)$ used in the denominator of Eq. 1 is the Hankel function of second kind defined as

$$H_n^{(2)}(x) = J_n(x) - jN_n(x),\qquad(8)$$

where $J_n(x)$ and $N_n(x)$ are Bessel functions of the first and second kind, respectively, and are defined by infinite series that can be found in standard references.[4,5] The function $\dot{H}_n^{(2)}(x)$ used in the denominators of Eqs. 2 and 7 is the derivative of $H_n^{(2)}(x)$ with respect to x, and is related to $H_n^{(2)}(x)$ and $H_{n+1}^{(2)}(x)$ by the equation:

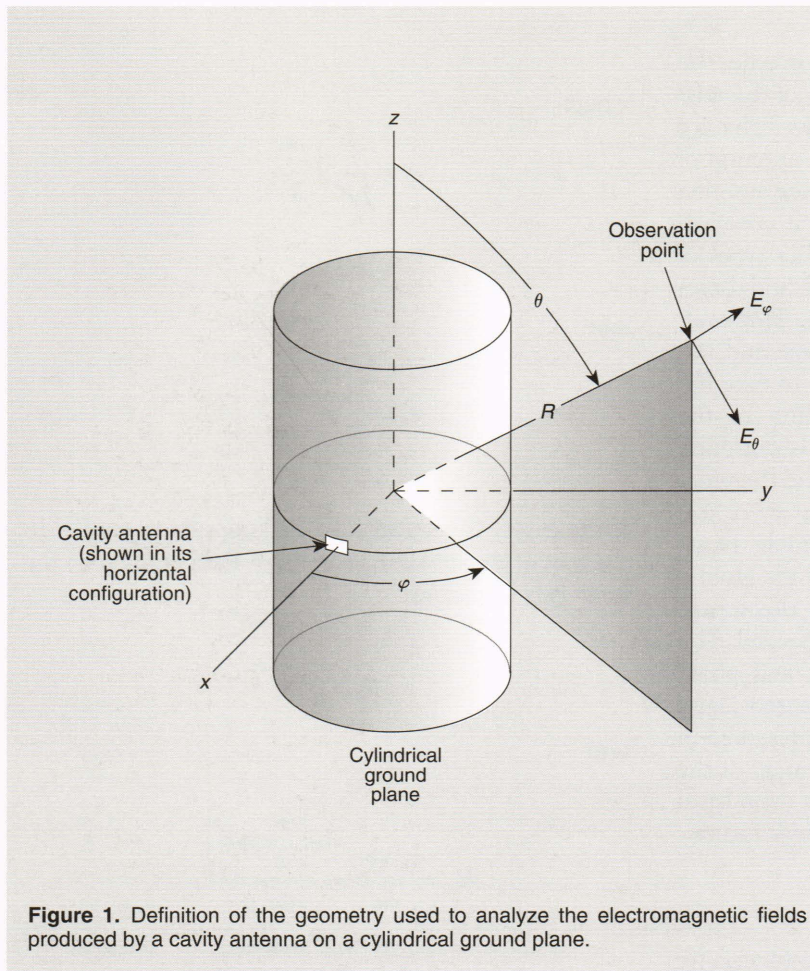$$\dot{H}_n^{(2)}(x) = \frac{n}{x}H_n^{(2)}(x) - H_{n+1}^{(2)}(x).\qquad(9)$$

When Reference 3 was written, the $J_n(x)$ and $N_n(x)$ functions were normally evaluated by laborious interpolation of printed tables. Now, however, it is quite feasible to evaluate them for the exact values of x needed for the analytical job at hand using desktop computers and finite approximations of the defining series. In this article, an algorithm called *besselh*, which is provided in a commercially available analysis package called MATLAB, was used to generate $H_n^{(1)}(x)$, which is the complex conjugate of the $H_n^{(2)}(x)$ functions needed in Eqs. 1 and 9.

MATLAB functions called *Hcavity* and *Vcavity*, for computing the E fields produced by horizontally and vertically oriented cavity antennas, are shown in Figs. A and B, respectively, in the boxed insert entitled MATLAB Functions. The *CnvrtLin* function shown in Fig. C converts these complex E-field components into arrays that give the equivalent power gain and phase of the cavity antennas when measured with an appropriately oriented, linearly polarized receiving antenna. The *CnvrtCir* function, also shown in Fig. C, converts the complex components of the E_θ and E_φ fields produced by a horizontal cavity into arrays that give the equivalent power gain and phase of the cavity when it is measured with a left- or right-hand circularly polarized (LHCP or RHCP) receiving antenna. This operation is accomplished by using either

$$E_{\text{LHCP}} = \frac{1}{2}\left(E_\varphi + jE_\theta\right)\qquad(10)$$

or

$$E_{\text{RHCP}} = \frac{1}{2}\left(E_\varphi - jE_\theta\right)\qquad(11)$$

to calculate the real and imaginary components of the desired circular E field, and then converting those components into equivalent power gain and phase. The *CnvrtLin* routine uses the expression

$$G = 10\log_{10}\left(0.5\left|E_{\text{Lin}}\right|^2\right)\qquad(12)$$

to generate the equivalent power gain of the linear field components, E_θ or E_φ, whereas the *CnvrtCir* routine uses the expression

Figure 1. Definition of the geometry used to analyze the electromagnetic fields produced by a cavity antenna on a cylindrical ground plane.

MATLAB FUNCTIONS

Shown in the following figures are MATLAB functions used to generate complex arrays representing the electromagnetic fields, E_θ and E_φ, produced by horizontally and vertically oriented cavity antennas on cylindrical ground planes. Also shown are functions that convert these complex arrays to real arrays representing the gain and phase properties of these antennas.

```
function [E1,E2]=Hcavity(Theta,Phi,ka)
%
% This function calculates the E field produced by a horizontal (circumferentially-oriented)
% cavity-backed antenna mounted on a long cylinder of radius 'a'. 'E1' and 'E2' will be (mxn)-
% dimensional arrays giving the Theta and Phi components of the E field at the set of observa-
% tion points specified by the m-element column vector 'Theta' and the n-element row vector
% 'Phi'. The parameter 'ka' must be set equal to 2*pi*f*a/c, where: f=frequency(Hz) and
% c=speed-of-light. 'a' and 'c' must be in consistent units (e.g., meters & m/sec), and 'Theta'
% & 'Phi' must be supplied in units of degrees.
%
Ph=pi*Phi/180; B=pi/(2*ka); Th=pi*Theta/180; Sth=sin(Th); X=ka*Sth; kasq=ka*ka;
Hk=conj(besselh(0,X)); Hl=conj(besselh(1,X)); S1=(1e0./(ka*Hk))*ones(1,N); S2=zeros(M,N);
Kmax=floor(2*ka); M=length(Theta); N=length(Phi);
%
for k=1:Kmax
   Hk=Hl; Hl=conj(besselh(k+1,X));
   T1=(j^k./Hk)*cos(k*Ph); T2=(j^k./((Hk./X)-(Hl/k)))*sin(k*Ph);
   F=2*ka*cos(k*B)/(kasq-k^2); S1=S1 + F*T1; S2=S2 + F*T2;
end
E1=((-j./Sth)*ones(1,N)).*S1; E2=((-j./(X.*tan(Th)))*ones(1,N)).*S2;
```

Figure A. MATLAB routine (*Hcavity*) for generating the real and imaginary components of the E fields, E_θ and E_φ, produced by a horizontally oriented cavity antenna on a cylindrical ground plane.

```
function Ephi=Vcavity(Theta,Phi,ka)
%
% This function calculates the E field produced by a vertical (axially-oriented) cavity-backed
% antenna mounted on a long cylinder of radius 'a'. 'Ephi' will be a (mxn)-dimensional array
% giving the E field at the set of observation points specified by the m-element column vector
% 'Theta' and the n-element row vector 'Phi'. The parameter 'ka' must be set equal to 2*pi*f*a/
% c, where: f=frequency(in Hz) and c=speed-of-light. 'a' and 'c' must be in consistent units
% (e.g., meters & m/sec), and 'Theta' & 'Phi' must be supplied in units of degrees.
%
Kmax=floor(2*ka); Ph=pi*Phi/180; N=length(Phi); Th=pi*Theta/180; Sth=sin(Th); X=ka*Sth;
Hl=conj(besselh(1,X)); S=-(1e0./Hl)*ones(1,N);
%
for k=1:Kmax
   Hk=Hl; Hl=conj(besselh(k+1,X)); T=j^k./((k*Hk./X)-Hl); S=S + 2*T*cos(k*Ph);
end
Ephi=((cos(0.5*pi*cos(Th))./(X.*Sth))*ones(1,N)).*S;
```

Figure B. MATLAB routine (*Vcavity*) for generating the real and imaginary components of the E field, E_φ, produced by a vertically oriented cavity antenna on a cylindrical ground plane.

$$G = 10\log_{10}|E_{\text{Cir}}|^2 \qquad (13)$$

to generate the equivalent power gain of the circular fields, E_{LHCP} or E_{RHCP}. These expressions produce gain values that have the correct shape relative to variations in the line-of-sight angles θ and φ, but they are incorrectly biased because the input impedance of the cavity as well as the impedance of space at the observation point have not been taken into account. This bias

can be removed through proper adjustment of the V_0 constant.

The phase values produced by the *CnvrtLin* and *CnvrtCir* functions are the so-called "partial phase" values, obtained by taking the principal two-argument arctangent of the real and imaginary parts of whichever E field component is of interest. Since the principal arctangent is constrained to the range of values between $-180°$ and $+180°$, plots of the partial phase function along most θ or φ cuts have numerous $360°$

MATLAB FUNCTIONS (continued)

```
function [Gain,Phase]=CnvrtLin(VGMap)
%
%  This function converts linearly polarized antenna voltage-gain arrays to power-gain & phase
%  form.
%
Gain=10*log10(1e-10 + 0.5*real(VGMap.*conj(VGMap))); Phase=(180/pi)*angle(VGMap);


function [Gain,Phase]=CnvrtCir(VG1,VG2,P)
%
%  This function converts complex 2-axis antenna voltage-gain arrays to arrays of equivalent
%  power-gain and phase relative to a LHCP or RHCP reference antenna. 'P'={1|-1} for left or
%  right polarization. 'VG1' and 'VG2' are (m,n)-dimensional arrays of complex voltage gains for
%  the theta and phi components of the E field produced by a horizontal cavity.
%
VGCir=0.5*((real(VG2)-P*imag(VG1))+j*(imag(VG2)+P*real(VG1)));
Gain=10*log10(real(VGCir.*conj(VGCir))); Phase=(180/pi)*angle(VGCir);
```

Figure C. MATLAB routines (*CnvrtLin* and *CnvrtCir*) for converting the real and imaginary field values produced by the *Hcavity* and *Vcavity* routines to two-dimensional arrays giving the equivalent gain and phase of the cavity antennas.

```
function Tph=FrntWrp(Pph);
%
%  This function removes 360-degree discontinuities in the input partial phase map 'Pph' of an
%  antenna. It first unwraps the theta-sweep at phi=0, and it then unwraps all phi-sweeps (for
%  each theta value), starting at phi=0 and sweeping right to phi=180 and left to phi=-178.
%
Tph=Pph; [M,N]=size(Pph); I=[2:M]; J=[2:N/2]; K=[N:-1:1+N/2]; L=[1,N:-1:2+N/2];
Tph(I,1)=Tph(I,1)-cumsum(360*floor(0.5+(Tph(I,1)-Tph(I-1,1))/360));
Tph(:,J)=Tph(:,J)-cumsum(360*floor(0.5+(Tph(:,J)-Tph(:,J-1))'/360))';
Tph(:,K)=Tph(:,K)-cumsum(360*floor(0.5+(Tph(:,K)-Tph(:,L))'/360))';


function Tph=HHWrp(Pph);
%
%  This function removes 360-degree discontinuities in the input partial phase map 'Pph' of an
%  antenna. It first unwraps the phi-sweep at theta=0, and it then unwraps all theta-sweeps (for
%  each phi value), starting at theta=0 and sweeping up to theta=180. A special 360 deg adjust-
%  ment is then added to the upper center region to correct for unwrapping errors resulting from
%  finite 2 deg sampling.
%
Tph=Pph; [M,N]=size(Pph); I=[2:M]; J=[2:N]; K=[46:89]; L=[47:135];
Tph(1,J)=Tph(1,J)-cumsum(360*floor(0.5+(Tph(1,J)-Tph(1,J-1))'/360))';
Tph(I,:)=Tph(I,:)-cumsum(360*floor(0.5+(Tph(I,:)-Tph(I-1,:))/360));
Tph(K,L)=360+Tph(K,L);
```

Figure D. MATLAB routines (*FrntWrp* and *HHWrp*) for removing 360° discontinuities in the partial phase data produced by the routines *CnvrtCir* and *CnvrtLin*.

discontinuities in them. These are removed, to the extent possible, with two phase-unwrapping routines called *FrntWrp* and *HHWrp*, which are shown in Fig. D. The phase data obtained from these phase-unwrapping operations are usually called "total phase."

NUMERICAL RESULTS

Complex arrays representing E_θ and E_ϕ, and real arrays representing the gain and phase values corresponding to these fields, were computed for both horizontally and vertically oriented cavity antennas over a grid of $\{\theta,\varphi\}$ pairs generated by the sets $\theta = $ $\{2°, 4°, \ldots, 178°\}$ and $\varphi = \{0°, 2°, \ldots, 358°\}$, respectively. Three-dimensional perspective plots exhibiting the gain and phase properties of these antennas were then produced. Figures 2 and 3 show the gain and phase of the E_θ and E_φ fields generated by a horizontally oriented cavity, and Fig. 4 shows a similar pair of plots for the E_φ field generated by a vertically oriented cavity.

The gain plots shown in Figs. 2 and 4 exhibit a gradual reduction in gain as φ increases from 0° to 180°. This is contrary to what a simple line-of-sight model predicts, viz., a sudden loss of gain at $\varphi = 90°$ due to the loss of visibility at that angle. Figure 2 shows that
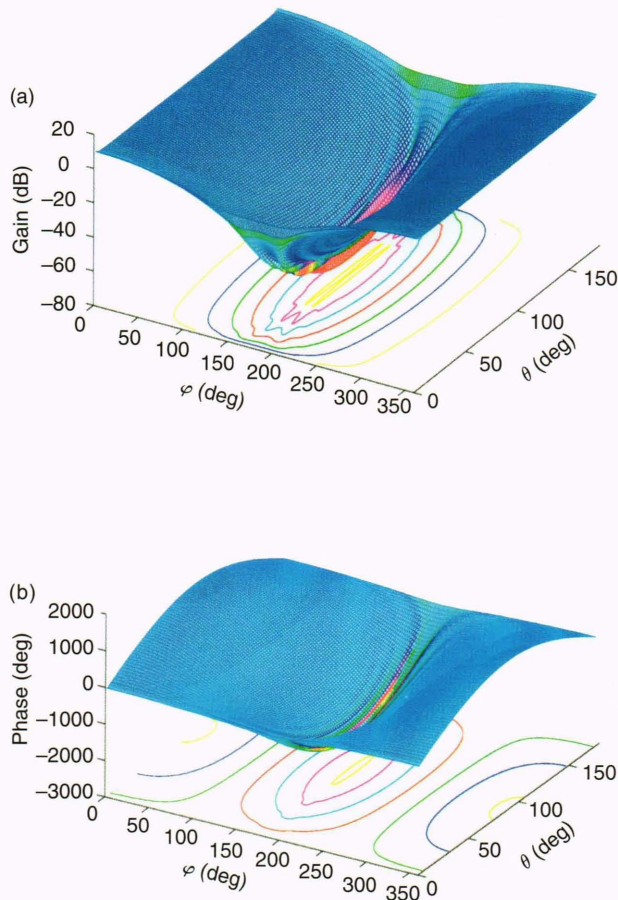
Figure 2. Gain (a) and phase (b) of a horizontal cavity using a vertically polarized reference antenna located at azimuth angle φ and elevation angle θ relative to the cylinder coordinate frame.
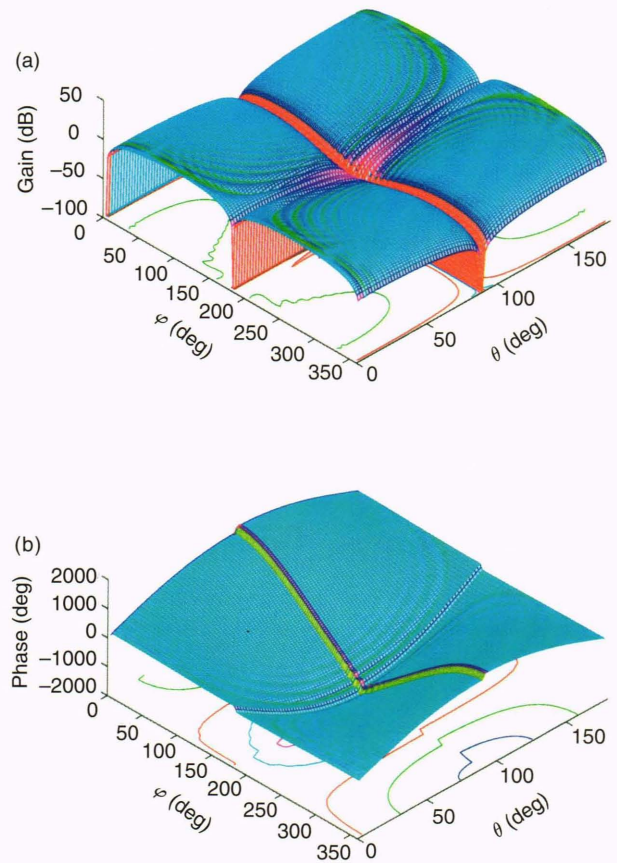
Figure 3. Gain (a) and phase (b) of a horizontal cavity using a horizontally polarized reference antenna located at azimuth angle φ and elevation angle θ relative to the cylinder coordinate frame.

the horizontal cavity has nearly constant gain in the vicinity of $\varphi = 0°$ as θ varies from $0°$ to $180°$. On the other hand, Fig. 4 shows that the gain of the vertical cavity in the same vicinity varies considerably as θ varies from $0°$ to $180°$, with maximum gain occurring at $\theta = 90°$ and gain nulls occurring at $\theta = 0°$ and $\theta = 180°$ (the nose and tail directions, respectively). Both orientations of the cavity show some "up and down" rippling of the gain pattern as φ approaches $180°$, although the effect is more pronounced for the vertical cavity than for the horizontal cavity. This effect is due to interference between the wave propagating around the cylinder in the positive-φ direction and the wave propagating around the cylinder in the negative-φ direction. The gain pattern shown in Fig. 3 for the φ component of the field generated by a horizontal cavity is substantially different in character from the other two cases. In this case, the gain has infinitely deep nulls at $\varphi = 0°$, $\varphi = 180°$, and $\theta = 180°$ and relatively constant gain elsewhere.

The phase patterns shown in Fig. 2 for the E_θ field generated by a horizontal cavity and in Fig. 4 for the E_φ field generated by a vertical cavity were obtained

by applying the *FmtWrp* routine to the partial phase arrays pertaining to these two fields. The phase patterns are remarkably similar in shape; both of them show a positive peak at $\{\theta = 90°, \varphi = 0°\}$, a negative peak at $\{\theta = 90°, \varphi = 180°\}$, and a difference between them of $\approx 3000°$. In addition, they are both quite smooth relative to variations in θ and φ at all points except those that are near $\varphi = 180°$. At those points, a contouring effect is evident where the phase holds relatively constant at several different plateau levels. The plateaus are separated by regions of rapid change in which the phase shifts up or down by approximately $180°$. It can also be shown that the regions of rapid phase change are the regions where the gain plots have deep nulls. The phase pattern shown in Fig. 3 for the φ component of the field generated by a horizontal cavity was obtained by applying a different unwrapping routine (viz., *HHWrp*) to the partial phase array pertaining to that field. This phase pattern is generally similar in shape to the phase patterns shown in Figs. 2 and 4, but there are instantaneous $180°$ "cliffs" at $\varphi = 0°$, $\varphi = 180°$, and $\theta = 180°$ (the same points at which the gain nulls occur), and a different unwrapping

routine, as well as a little bit of "hand tailoring," was required to correctly generate the total phase map for this case.

The gain and phase patterns of a horizontal cavity, when observed with an LHCP reference antenna, are shown in Fig. 5. The data in this case are obtained by (1) applying the *CnvrtCir* function to the E_θ and E_φ arrays generated by *Hcavity*, and then (2) applying *FrntWrp* to the partial phase data to obtain the total phase data shown in Fig. 5. A gain null again occurs along the θ cut at $\varphi = 180°$, so a 180° phase cliff is observed along this line. In addition, there are two short φ-cut segments near the center of the plot where the gain is very nearly zero, and the phase changes quite rapidly along these two lines as well.

SIMPLIFIED PHASE MODEL

Additional insight into the behavior of cavity antennas on cylindrical ground planes is obtained by examining plots of total phase vs. φ for various θ angles. Examples of such plots are shown in Fig. 6a for the case of E_θ produced by a horizontal cavity and Fig.

6b for the case of E_φ produced by a vertical cavity. Note that the curves are basically sinusoidal in the regions $0° \leq \varphi \leq 90°$ and $270° \leq \varphi \leq 360°$ and V-shaped in the region $90° \leq \varphi \leq 270°$. This result suggests that a simplified model for the total phase of these field components is obtained by multiplying the wavenumber k by the difference between the length of the shortest path from the antenna to the observation point, and R (the distance of the observation point from the origin of the coordinate frame). When the observation point is visible to the cavity antenna, i.e., when $0° \leq \varphi \leq 90°$ or $270° \leq \varphi \leq 360°$, this model results in the equation

$$\psi(\theta, \varphi) = B + \left(180°/\pi\right) ka \sin\theta \cos\varphi \qquad (14)$$

for the total phase in degrees of the cavity antenna, where B is a phase bias term that may be needed. However, when the observation point is obscured by the cylinder, i.e., when $90° \leq \varphi \leq 270°$, the shortest path must be one that does not penetrate the surface
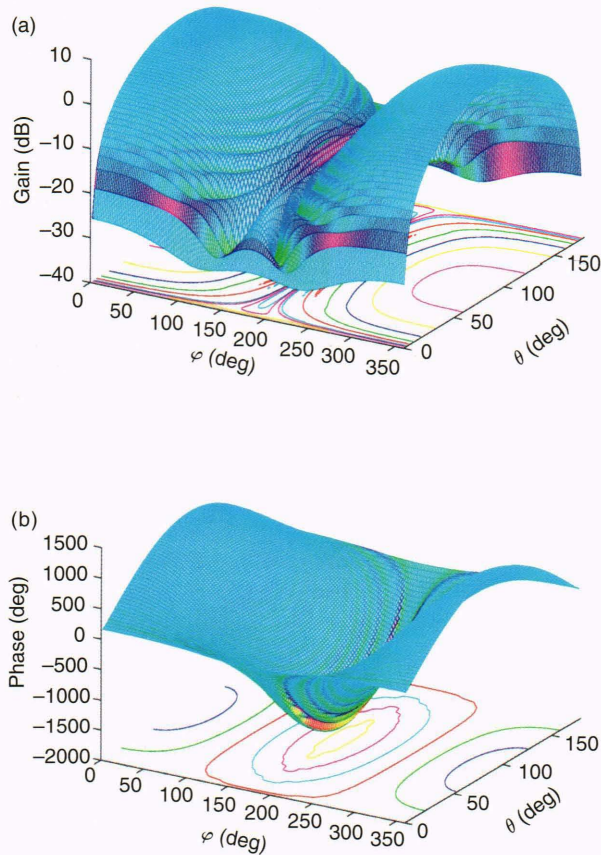

Figure 4. Gain (a) and phase (b) of a vertical cavity using a horizontally polarized reference antenna located at azimuth angle φ and elevation angle θ relative to the cylinder coordinate frame.
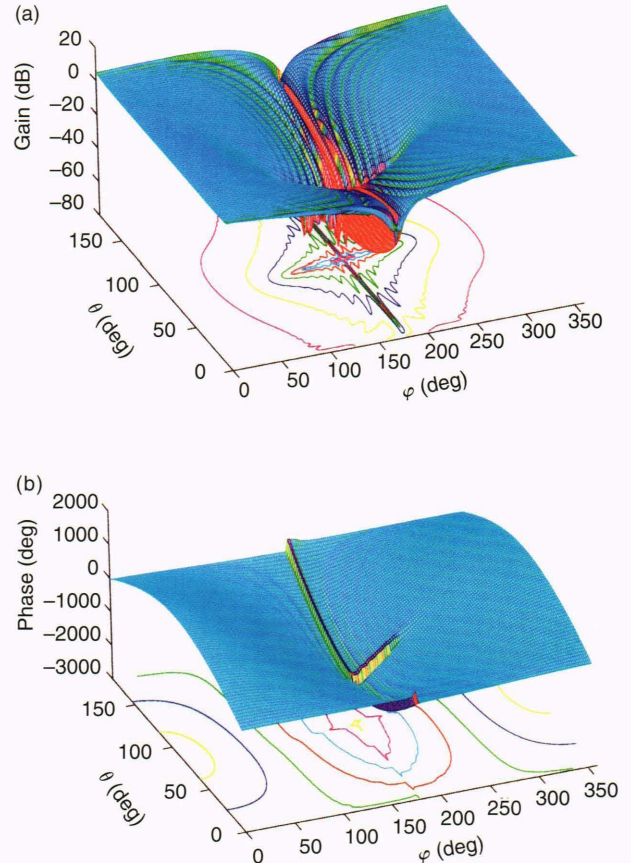
Figure 5. Gain (a) and phase (b) of a horizontal cavity using an LHCP reference antenna located at azimuth angle φ and elevation angle θ relative to the cylinder coordinate frame.
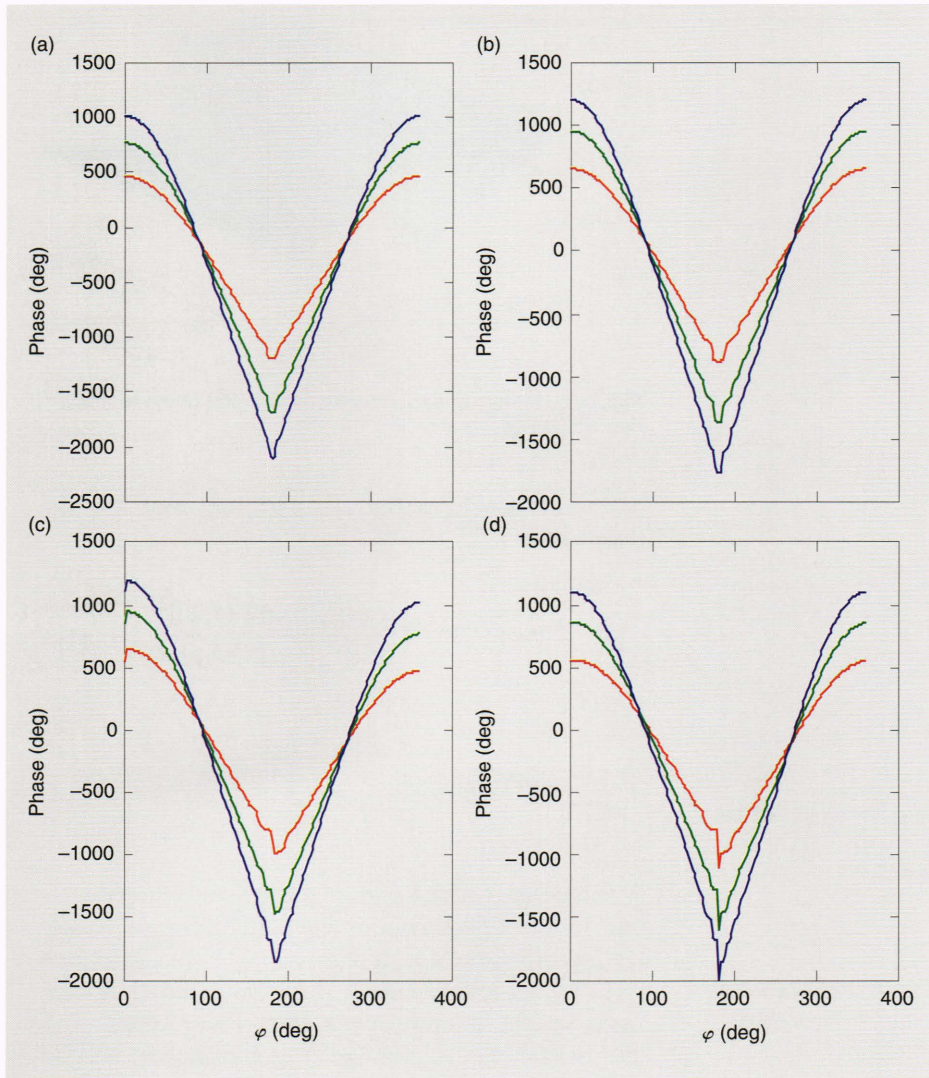
Figure 6. Total phase of (a) E_θ field generated by a horizontal cavity, (b) E_φ field generated by a vertical cavity, (c) E_φ field generated by a horizontal cavity, and (d) E_{LHCP} field generated by a horizontal cavity. (Red curves: $\theta = 30°$, green curves: $\theta = 60°$, and blue curves: $\theta = 90°$.)

of the metallic cylinder, and therefore consists of a spiral segment and a straight-line segment as shown in Fig. 7. The spiral starts at $\varphi = 0°$, proceeds along the surface of the cylinder with an inclination of $90° - \theta$, and terminates at $\varphi - 90°$ (if $90° \leq \varphi \leq 180°$) or $\varphi + 90°$ (if $180° \leq \varphi \leq 270°$). At this point the shortest path continues as a straight line proceeding from the previously defined terminal point of the spiral to the observation point. It can be shown that the difference between the length of this path and R approaches

$$\Delta\rho = (\pi/180°)\big[90° - abs(\varphi - 180°)\big]a\sin\theta \quad (15)$$

in the limit as $R \to \infty$. Therefore, a combined simplified model for the phase of E_θ produced by a horizontal cavity and/or E_φ produced by a vertical cavity is provided by the following equation:

$$\psi(\theta,\varphi) = B + \begin{cases} (180°/\pi)ka\sin\theta\cos\varphi, & \cos\varphi \geq 0 \\ -[90° - abs(\varphi - 180°)]ka\sin\theta, & \cos\varphi < 0 \end{cases}$$

$$(16)$$

where the bias B is equal to $-90°$ for a horizontal cavity or $+90°$ for a vertical cavity.

Construction of a simplified phase model for the E_φ field produced by a horizontal cavity is somewhat more complex. The curves shown in Fig. 6c demonstrate that Eq. 15 can still be used, but a single bias value cannot be used for all values of θ and φ. Instead, different values must be used depending on where the point representing θ and φ falls in the θ,φ plane. These values are listed in Table 1. Approximation of the total phase of the LHCP or RHCP components of the field generated by a horizontal cavity is even more involved. The LHCP case is shown in Fig. 6d. An approximation that works reasonably well is given by the equation
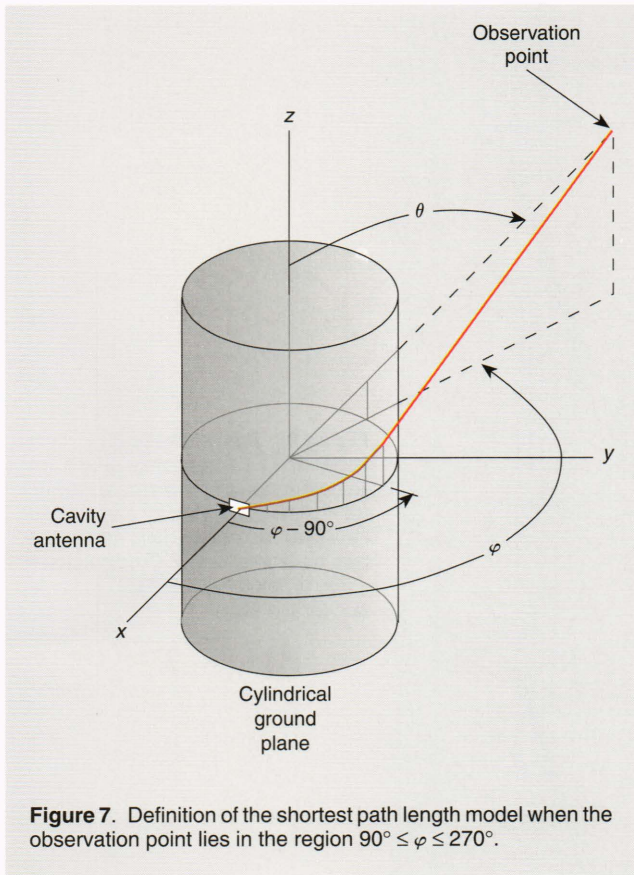
Figure 7. Definition of the shortest path length model when the observation point lies in the region $90° \leq \varphi \leq 270°$.

Table 1. Bias values, B, required in Eq. 16 to approximate the phase of the E_φ field generated by a horizontally oriented cavity.

$\theta \backslash \varphi$-Regions	$0° < \varphi < 180°$	$180° < \varphi < 360°$
$0° \leq \theta < 90°$	$+90°$	$-90°$
$90° < \theta \leq 180°$	$+270°$	$+90°$

$$\psi(\theta,\varphi) = B \pm T(\theta,\varphi) + \begin{cases} (180°/\pi)ka\sin\theta\cos\varphi \\ -[90° - \mathrm{abs}(\varphi - 180°)]ka\sin\theta \end{cases}$$

$$(17)$$

where for the LHCP case, $B = 0°$ and $+T(\theta,\varphi)$ is used, and for the RHCP case, $B = -180°$ and $-T(\theta,\varphi)$ is used. The conditions for the terms to the right of the brace are the same as those given in Eq. 16. The term $\pm T(\theta,\varphi)$ models an effect called "twist," which is the rotation of the plane of polarization of the E field as the observation point is moved from its initial $\{0°,0°\}$ position to its final $\{\theta,\varphi\}$ position. An equation describing this effect can be derived by treating the E field as elliptically polarized and solving for the angle between the θ axis and the semimajor axis of this field. This
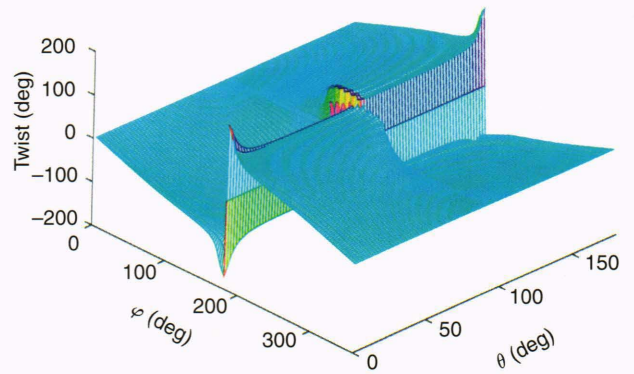

Figure 8. Three-dimensional perspective plot of the twist effect defined by Eqs. 18 and 19.

procedure generates the following equation for the twist effect:

$$T(\theta,\varphi) = \tan^{-1}\left\{\frac{\mathrm{real}[E_\varphi(\theta,\varphi)W(\theta,\varphi)]}{\mathrm{real}[E_\theta(\theta,\varphi)W(\theta,\varphi)]}\right\}, \quad (18)$$

where

$$W(\theta,\varphi) = \exp\left[-j\frac{1}{2}\mathrm{angle}\left(\frac{E_\theta^2 + E_\varphi^2}{2}\right)\right]. \quad (19)$$

A three-dimensional plot of the twist effect given by Eqs. 18 and 19 is shown in Fig. 8. (The function angle (z) used in Eq. 19 is defined as $\tan^{-1}$ [imag (z)/real (z)].) Notice that φ cuts of the $T(\theta, \varphi)$ function have jumps of 180° or more at $\varphi = 180°$. These jumps result in a net buildup in phase of 0° as φ varies from 0° to 360°. However, when phase-sensitive circuits (such as phase-locked loops) process these signals, they are very likely to exhibit a one-cycle per turn buildup in phase, particularly at θ close to 0° or 180°, because noise effects frequently cause jumps of the opposite sign to occur at $\varphi = 180°$.

Residuals between the true phase of the cavity antennas and the simplified models defined here are shown in Fig. 9. The simplified models are all accurate to 10° or better when $|\varphi| \leq 65°$. This accuracy demonstrates that the cavity antennas are fairly well approximated as point phase centers when the line of sight to the receiving antenna is well into the unobscured region of the cylindrical ground plane. However, when $|\varphi| > 65°$, the magnitude of the residuals increases rapidly above the 10° level, typically to 200°–300°. This increase occurs probably because the "electrical radius" of the cylinder as the waves propagate around it is not necessarily equal to the physical radius of the cylinder. However, additional work is required to confirm this speculation. The residuals shown in Fig. 9 have rapid, high-amplitude oscillations around $\varphi = 180°$ caused by interference between the waves
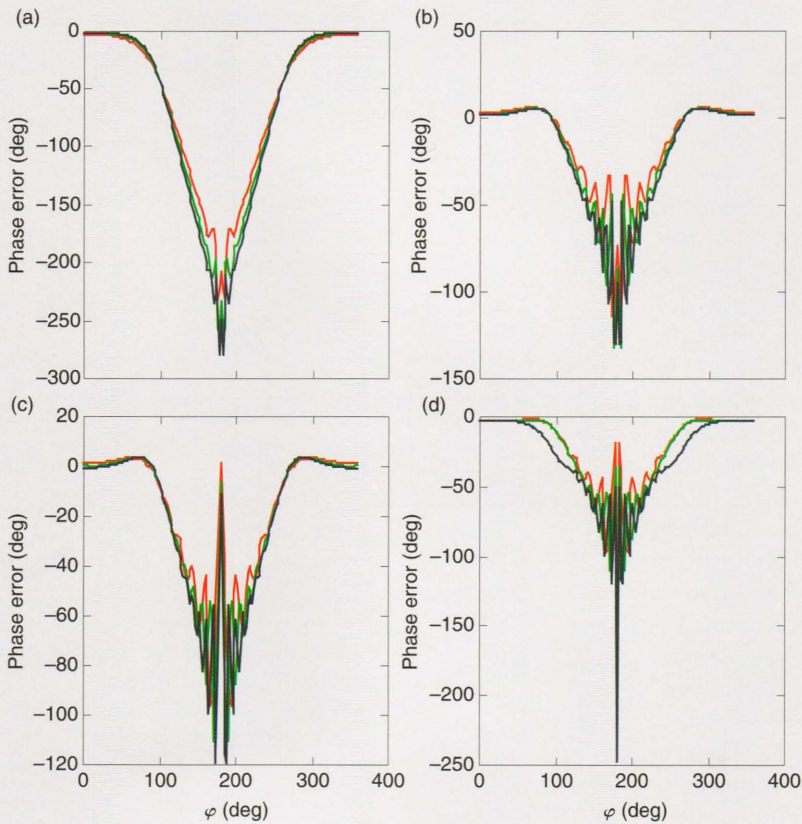
Figure 9. Phase errors due to the shortest path length model. (a) E_θ field/horizontal cavity, (b) E_φ field/vertical cavity, (c) E_φ field/horizontal cavity, (d) E_{LHCP} field/horizontal cavity. (Red curves: $\theta = 30°$, green curves: $\theta = 60°$, and blue curves: $\theta = 75°$.)

propagating in opposite directions around the cylinder. Accurate modeling of these oscillations is difficult because small changes in a, θ, and φ cause big changes in the corresponding phase residual.

EXPERIMENTAL RESULTS

One of APL's responsibilities for the Advanced Interceptor Technology program was to provide payload equipment for a missile to be used as a target vehicle for an interceptor built by the Martin-Marietta Corporation. Figure 10 shows the missile and the antenna arrangement. The purpose of the payload equipment was to enhance the thermal signature of the vehicle and provide data enabling the miss distance and point of closest approach of the interceptor's path past the target to be estimated. A system called the Miss Distance Measurement System (MDMS) was developed to address the latter requirement. This system has two main subsystems: a two-translator Satrack system for measuring the absolute and relative
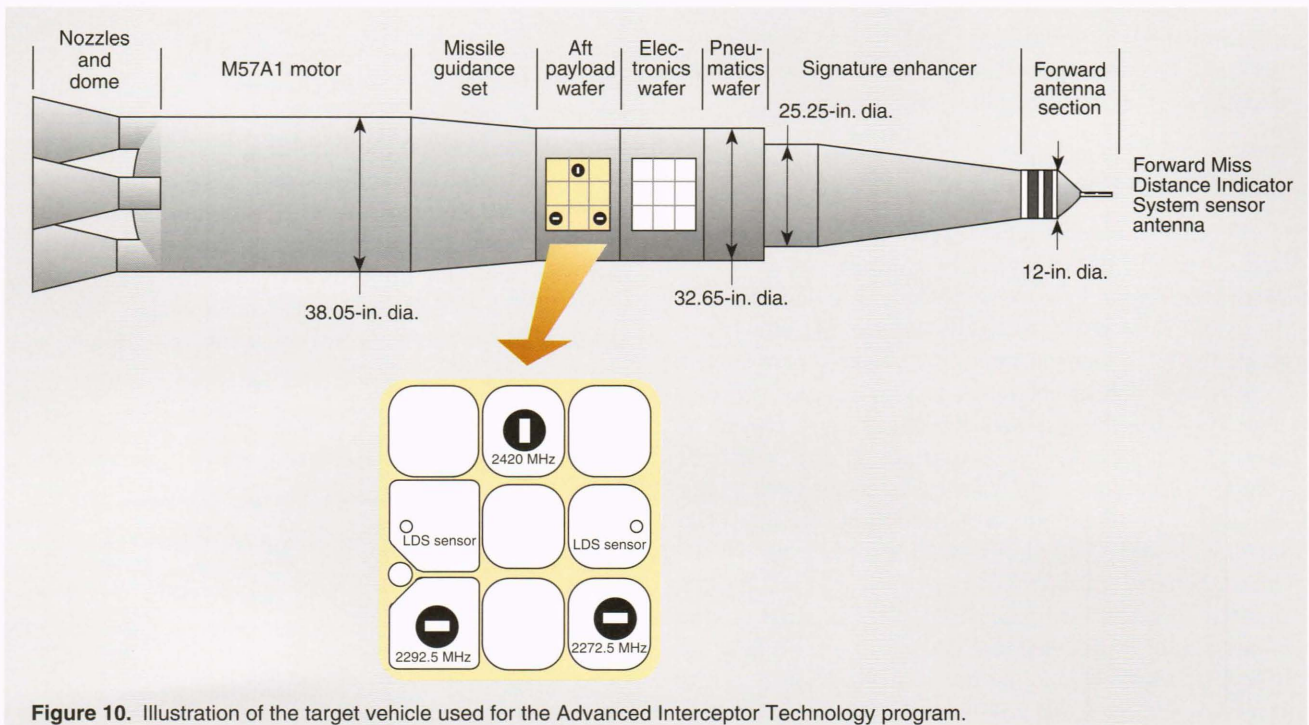

Figure 10. Illustration of the target vehicle used for the Advanced Interceptor Technology program.

trajectory of each vehicle, and a short-range radar system called the Miss Distance Indicator System (MDIS), located in the target vehicle, for independently measuring the point of closest approach.

The MDIS uses the shape of the Doppler shift in the returned pulses to measure the miss distance between the interceptor's trajectory and each of four cavity-type antennas on the target vehicle, and it is therefore sensitive to the phase characteristics of those antennas. The software that processes the data produced by the missile-borne sensors assumes that these antennas can be modeled as single-point phase centers. However, there were numerous constraints on where the antennas could be located, and some of them ended up having to be on small ground-plane panels inserted into a 3 × 3 array of skin openings behind a deployable door (see the enlarged area in Figure 10).

Uncertainties about the effect of this ground-plane arrangement led to concern that the antennas might be very poorly approximated as single-point phase centers. Therefore, the antennas and ground planes were installed on a mock-up of the aft payload wafer, and the gain and phase properties of the assembly were measured in APL's Antenna and Bore-Sight Test Facility. Some results of that test are shown in Fig. 11. The two curves in the gain plot show the gain of the horizontally oriented sensor antenna and the vertically oriented telemetry antenna at $\varphi = 0°$ as θ varies from 0° to 180°. Note that the horizontal cavity has relatively constant gain over this range, whereas the gain of the vertical cavity varies considerably. The two curves shown in the phase plot demonstrate the phase properties of these two antennas at $\theta = 90°$ as φ varies from $-180°$ to $+180°$. Note that these curves do show the sinusoidal and V-shaped properties described in the previous section, and the phase contouring effects are also obvious, particularly for the vertically oriented cavity.

CONCLUSIONS

The electromagnetic fields produced by horizontally and vertically oriented cavity antennas attached to cylindrical ground planes are ideally described by Eqs. 1, 2, and 7. Various physically measurable effects are predicted by these equations: phase behavior consistent with a well-defined phase center when the cavity is well into the unobscured region of the cylindrical ground plane, gradual gain attenuation and V-shaped phase vs. φ behavior when the cavity is obscured by the cylindrical ground plane, and interference between the clockwise and counterclockwise propagating waves when the receiving antenna is near the $\varphi = 180°$ point. Simplified phase models based on the single-point phase center assumption are correct to within ±10° of electrical phase for all unobscured observation points out to $\varphi \approx ±65°$. At that point the errors begin to grow
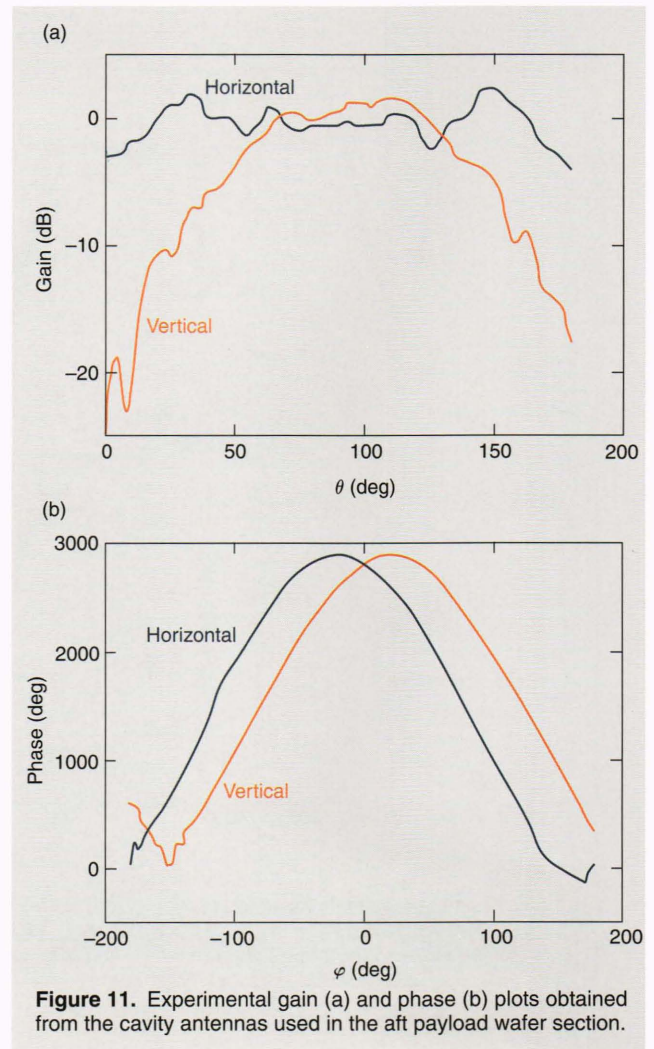

Figure 11. Experimental gain (a) and phase (b) plots obtained from the cavity antennas used in the aft payload wafer section.

and reach values of more than 100° near $\varphi = 180°$. However, these approximation errors might be reduced with further work on the simplified models. The results obtained from this analysis can also be used as a reference for comparison with gain and phase data obtained from physical antenna systems. This comparison was made for the sensor and telemetry antennas chosen for the MDIS, which was developed by APL for the Advanced Interceptor Technology program.

REFERENCES

[1] Hofmann-Wellenhof, B., *Global Positioning System/Theory and Practice*, 2nd ed., Springer-Verlag, New York (1993).
[2] Balanis, C. A., *Antenna Theory/Analysis and Design*, Harper & Row Publishers, New York (1982).
[3] Bailin, L. L., "The Radiation Field Produced by a Slot in a Large Circular Cylinder," *IRE Trans. Antennas Propag.* **AP-3(3)**, 128–137 (1955).
[4] Harrington, R. F., *Time Harmonic Electromagnetic Fields*, Appendix D, McGraw-Hill, New York (1961).
[5] Spanier, J., and Oldham, K. B., *An Atlas of Functions*, Hemisphere Publishing Corp., Washington, DC (1987).

THE AUTHOR

DENNIS J. DUVEN received B.S., M.S., and Ph.D. degrees in electrical engineering from Iowa State University in 1962, 1964, and 1971, respectively. He was an Assistant Professor in the electrical engineering department at Iowa State while working on his Ph.D. degree and taught numerous courses in automatic control and communication systems. Dr. Duven joined the APL Space Department in 1973 and began work on an advanced Global Positioning System (GPS) missile tracking system called Satrack I. In 1982, he was appointed system scientist for a follow-on GPS missile tracking system called Satrack II. That system is currently the baseline system for validating the accuracy of the Navy's Trident II missiles. Dr. Duven is Supervisor of the Satellite Control Systems Section of the Space Applications Group and is currently doing analytical work for the Boost-Phase Interceptor program and two IR&D projects. His e-mail address is Dennis.Duven@jhuapl.edu.